

Article

Photo-Tunable Azobenzene-Anthraquinone Schiff Base Copper Complexes as Mediators for Laccase in Biofuel Cell Cathode

Kazuto Kajiwara ¹, Sayantan Pradhan ², Tomoyuki Haraguchi ¹, Chittaranjan Sinha ², Rakesh Parida ³, Santanab Giri ⁴, Gourisankar Roymahaptra ⁴ and Takashiro Akitsu ^{1,*}

¹ Department of Chemistry, Faculty of Science, Tokyo University of Science, 1-3 Kagurazaka, Shinjuku-ku, Tokyo 162-8601, Japan; 1318527@ed.tus.ac.jp (K.K.); haraguchi@rs.tus.ac.jp (T.H.)

² Department of Chemistry, Jadavpur University, Kolkata, West Bengal 700032, India; sayantan.pradhan@saha.ac.in (S.P.); csinha@chemistry.jdvu.ac.in (C.S.)

³ Department of Chemistry, National Institute of Technology, Rourkela, Odisha 769008, India; 516cy6017@nitrkl.ac.in

⁴ Department of Applied Sciences, Haldia Institute of Technology, Haldia, West Bengal 721657, India; s giri.chem@hithaldia.in (S.G.); grm.chem@hithaldia.in (G.R.)

* Correspondence: akitsu2@rs.tus.ac.jp; Tel.: +81-3-5228-8271

Received: 13 April 2020; Accepted: 6 May 2020; Published: 11 May 2020



Abstract: Induced chirality (achiral target in chiral matrix such as proteins) sometimes play a useful role in evaluating supramolecular systems involving biomolecules. Enzymatic fuel cells, which generate electricity via enzymatic redox reactions at electrodes hold a significant potential for sustainable power. Bacterial laccase, a multi-copper oxidase, was used in the cathodic compartment of the enzymatic biofuel cells because of its low redox potential. Three new salen Cu(II) complexes were designed and investigated as mediators. The Schiff base ligands consisted of both a redox-active (anthraquinone) and a photochromic (azobenzene) moiety. The interaction between laccase and a mediator was examined with induced circular dichroism (CD) and the docking tool to observe in which of the laccase domains the mediators bind as well as study the photo-induced tuning of both the cis-trans photoisomerization and orientation by the Weigert effect. Both the electrochemical and photochromic properties are also discussed and compared using density functional theory (DFT), time-dependent (TD)-DFT, and docking simulations.

Keywords: enzymatic fuel cells; laccase; salen Cu(II) complex; docking; mediator; photo-tuning

1. Introduction

Laccase is an enzyme that catalyzes the four-electron reduction of oxygen to water through four copper atoms. A protein that includes copper atoms is referred to as multicopper oxidase [1–3]. The four copper atoms that are the active sites of the laccase are divided into three types (T1–T3) and T2 copper and the two T3 copper form triple nuclear clusters. T1 copper first receives electrons from the substrate and oxidizes the substrate, which is followed by a four-electron reduction at the T2 and T3 sites (Figure 1). Multicopper oxidase such as laccase is used as an enzyme on the cathode side of the enzyme-type biofuel cell [4–7]. Because biofuel cells use bio-based catalysts, they have the advantage to generate electricity at room temperature and low environmental load [8–10]. However, there is also a drawback that enzyme stability is lacking, and the electric power is smaller than that of other fuel cells. The following ways will be explored to solve the disadvantage of low power. A mediator that assists the donation and reception of the electron has been used for electron transfer between the

electrode and laccase [11–13]. A mediator is a substance that assists donating and receiving electrons and is sandwiched between an electrode and an enzyme [13].

To improve this electron transfer between the electrode and laccase, several types of metal complexes were investigated as mediators [14–20]. Molecular docking of suitable compounds (both ligands and complexes) to the hydrophobic pocket of laccase is useful to predict the distance or path of electron transfer and their effectivity in biofuel cells. For such hydrophobic weak interactions, induced chirality (namely characteristic CD bands) from chiral (asymmetric) protein matrix proteins sometimes play a useful role in evaluating a supramolecular interaction even for achiral guests. The presence of a noncoordinating, non-innocent substituent in the ligand backbone of the metal ligand or complex may be induced by the polarized UV-light to control the rate of redox processes [16,17]. In particular, the azobenzene moiety exhibits not only cis-trans photoisomerization but also the Weigert effect (molecular alignment induced by polarized UV light) [21], while controlling the molecular orientation for a suitable fitting. Herein, we designed new salen Cu(II) complexes as mediators. Generally, (chiral) salen metal complexes have been employed as (asymmetric) catalysis because of their advantage of stereochemical tuning (with respect to chirality) and redox properties with proper metal ions [22]. The Schiff base consisted of a redox-active (anthraquinone) [23–26] and photochromic (azobenzene) moiety [26–28]. Molecular docking [29] was conducted to investigate in which hydrophobic domain of the laccase the salen Cu(II) complexes are bound (Figure 2). Both electrochemical and photochromic properties were examined and compared with the density functional theory (DFT)/ time-dependent (TD)-DFT computed functions.

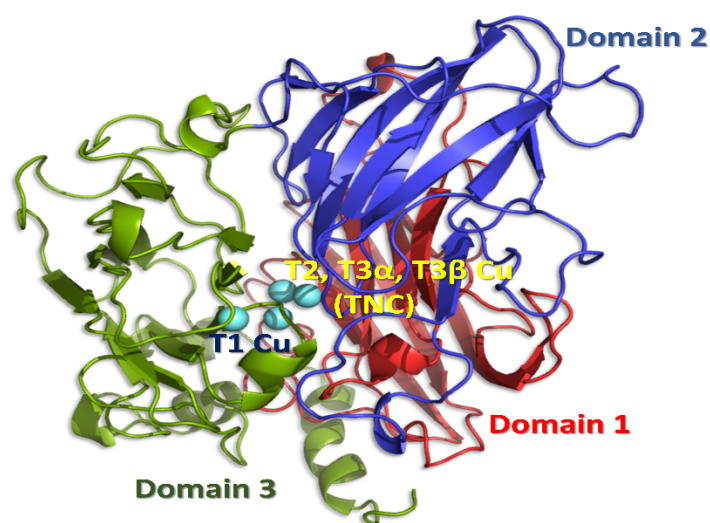


Figure 1. Structure of the enzyme, *Trametes versicolor* laccase (PDB ID: 1GYC), showing the three domains and the T1, T2, and T3 copper sites. Though laccase may form trimer assembly of three domains, each laccase molecule has one binding pocket.

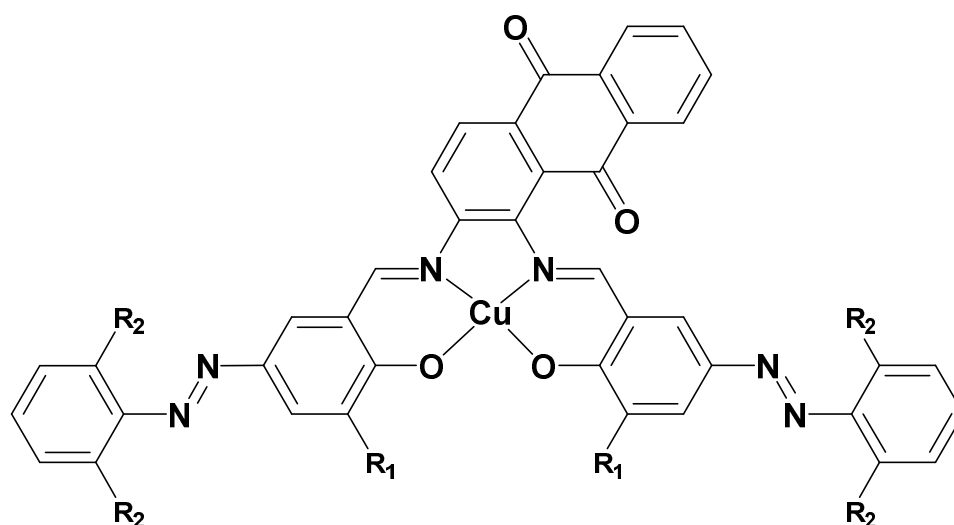


Figure 2. Structures of Cu(II) complexes **1–3**. (1) $R_1 = \text{OCH}_3$, $R_2 = \text{H}$, (2) $R_1 = \text{H}$, $R_2 = \text{H}$, and (3) $R_1 = \text{H}$, $R_2 = \text{Cl}$.

2. Materials and Methods

2.1. General Procedure

All chemicals of the highest commercial grade available (solvents from Kanto Chemical, Tokyo, Japan), organic compounds (Tokyo Chemical Industry, Tokyo, Japan), and metal sources and laccase (from *Trametes versicolor*) from Wako (Osaka, Japan) were used as received without further purification.

2.2. Preparations

2-Hydroxy-3-methoxy-5-phenyldiazobenzaldehyde, 2-hydroxy-5-phenyldiazobenzaldehyde, and 2,6-dichlorophenyl-2-hydroxy-5-phenyldiazobenzaldehyde (as precursors of **1–3**, respectively) were prepared according to the literature procedure using the corresponding precursor aldehydes [14]. The key reaction to form Schiff base is condensation of amine and aldehyde found by Hugo classically. Each of them (0.26 g, 1 mmol) was added to a methanol solution (80 mL) of 1,2-diaminoanthraquinone (0.12 g, 0.5 mmol) and stirred for 2 h at 318 K. Then $\text{Cu}(\text{CH}_3\text{COO})_2$ (0.1 g, 0.5 mmol) was added and stirred for 2 h at 318 K. A green crude product was obtained by filtration after evaporation and the product was recrystallized from hexane (less than 10 mL) and dried to yield **1–3**, respectively. Mass spectra could not be tried because of the lack of suitable solvents. Infrared (IR) and electronic (UV-vis) spectra are below.

1: Yield 48%. IR 1598 cm^{-1} s (C=N). UV-vis (DMSO) 280, 390, 450 nm, (reflectance) 460, 610 nm.

2: Yield 65%. IR 1586 cm^{-1} s (C=N). UV-vis (DMSO) 280, 390, 450 nm, (reflectance) 460, 610 nm.

3: Yield 11%. IR 1613 cm^{-1} s (C=N). UV-vis (DMSO) 270, 350, 540 nm, (reflectance) 460, 610 nm.

2.3. Physical Measurements

Infrared (IR) spectra were measured on a JASCO (Tokyo, Japan) FT-IR 4200 spectrophotometer in the range of $4000\text{--}400 \text{ cm}^{-1}$ at 298 K. (Polarized or normal) electronic (UV-vis) spectra were measured on a JASCO (Tokyo, Japan) V-650 spectrophotometer equipped with a polarizer in the range of $800\text{--}220 \text{ nm}$ at 298 K. Circular dichroism (CD) spectra were recorded on a JASCO (Tokyo, Japan) J-725 spectropolarimeter in the range of $800\text{--}200 \text{ nm}$ at 298 K. Electrochemical cyclic voltammetry (CV) were performed with a BAS (Tokyo, Japan) SEC2000—UV/vis and ALS2323 system with Ag/AgCl electrodes in the range of -0.50 to 0.80 V vs. Ag/Ag⁺. Photo-illumination of linearly polarized UV light was carried out using a lamp ($1.0 \text{ Mw}\cdot\text{cm}^{-2}$) by Hayashi Tokei (Tokyo, Japan) with optical filters

(UV, $\lambda = 200\text{--}400$ nm) by using optical fibers and a polarizer through optical filters (Sigma Koki, Tokyo, Japan).

2.4. X-ray Crystallography

Powder X-ray diffraction patterns of **1–3** were measured at 298 K using a CuK α source (about 0.154 nm) with Rigaku Smart Lab (Tokyo, Japan). The Rietveld analysis was carried out with a commercially available program package Rigaku PDXL2 ver.2.2.1.0 (Tokyo, Japan), by the following procedures: (measurement), indexing, cell and space group determination, input composition, and an initial structural model from DFT results, direct space method, addition of (isotropic) displacement parameters for non-hydrogen atoms, and refinement with hydrogen atoms under restraint. Although powder analysis generally may exhibit relatively high R_{wp} values, the purpose of crystal structures in this paper was not a closely quantitative discussion of bond distances nor angles but merely confirming newly prepared compounds mentioning overall structures.

Crystallographic data of **1**: $C_{42}H_{28}CuN_6O_6$, $Mw = 776.25$, $T = 298$ K, Triclinic, $P-1(\#2)$, $Z = 2$, $a = 11.756(18)$, $b = 16.051(19)$, $c = 11.189(13)$ Å, $\alpha = 81.22(8)$, $\beta = 83.61(7)$, $\gamma = 78.40(6)^\circ$, $V = 2037(5)$ Å³, $D = 1.266$ g·cm⁻³, $F(000) = 798$, $S = 6.8694$, $R_{wp} = 5.45\%$.

Crystallographic data of **2**: $C_{40}H_{24}CuN_6O_4$, $Mw = 716.20$, $T = 298$ K, Triclinic, $P-1(\#2)$, $Z = 2$, $a = 12.619(19)$, $b = 16.003(17)$, $c = 11.28(2)$ Å, $\alpha = 101.41(10)$, $\beta = 98.25(13)$, $\gamma = 110.70(8)^\circ$, $V = 2128(6)$ Å³, $D = 1.118$ g·cm⁻³, $F(000) = 734$, $S = 10.7396$, $R_{wp} = 7.63\%$.

Crystallographic data of **3**: $C_{40}H_{20}Cl_4CuN_6O_4$, $Mw = 853.97$, $T = 298$ K, Triclinic, $P-1(\#2)$, $Z = 2$, $a = 14.025(6)$, $b = 12.056(4)$, $c = 18.103(9)$ Å, $\alpha = 98.63(2)$, $\beta = 99.663(16)$, $\gamma = 102.33(2)^\circ$, $V = 2893(2)$ Å³, $D = 0.980$ g·cm⁻³, $F(000) = 862$, $S = 9.63$, $R_{wp} = 10.53\%$.

2.5. Computational Methods

Within the density functional theory framework, the B3LYP level of theory with an SDD basis set was used to optimize all the studied complexes. A vibrational frequency analysis was also performed to ensure the local minimum of the complexes. All the optimizations were done using the Gaussian 09W software Revision D.02 (Gaussian, Inc., Wallingford, CT, USA) [30]. To know the orbital information of the optimized structures, the TDDFT methodology, which is implemented in G09W, was used. Gaussian software was applied to calculate the density of the state (DOS) and partial DOS (PDOS). The solvent medium was incorporated with the polarizable continuum model (PCM). Docking of metal complexes was carried out with AutoDock 4.2.6 [31] on a Windows 10 platform with 8 GB RAM (random access memory) and Intel I 5 processor.

3. Results and Discussion

3.1. Structural Characterization of Complexes

All complexes **1–3** displayed a four-coordinated slightly distorted square planar *trans*-[N₂O₂] coordination geometry (which is in agreement with EPR of **2** and **3** in the solid state as $S = 1/2$ in the Supporting Information) and all atoms are located approximately within a plane, which suggests an extended conjugate system in the ligands. Figures 3–5 depict the crystal structures of **1–3**, respectively. Within the precision of the powder analysis, geometries of the organic ligand moiety exhibited normal values for the related compounds [17,32–34]. Overall structures (for example, around azo groups) were also similar to the density functional theory (DFT) optimized structures mentioned before. However, DFT optimized structures were not a complete square planar geometry but were somewhat distorted. Despite the photoisomerization of the azo groups, the salen skeleton and the organic ligands kept rigid structures. As the crystal structures indicate, the coordination in solutions of solvents is possible. Empty apical sites may potentially accept them in an axial position [35].

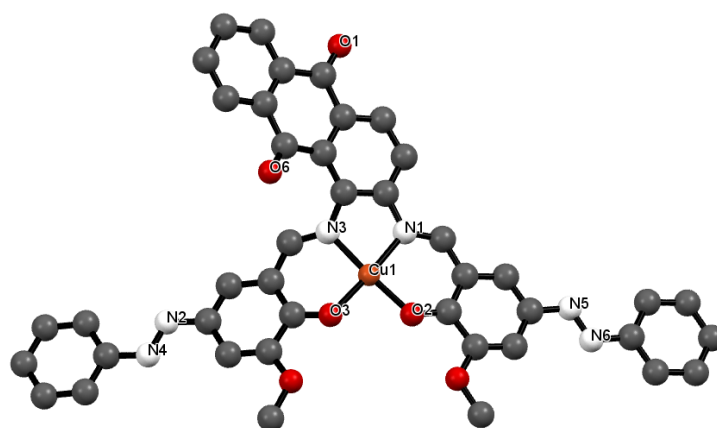


Figure 3. Crystal structure of **1** showing a selected atom labeling scheme. Selected bond lengths [Å] and angles [°] are as follows: Cu1-O2 = 1.854(2), Cu1-O3 = 1.885(3), Cu1-N1 = 1.957(3), Cu1-N3 = 1.913(2), N2-N4 = 1.2542(18), N5-N6 = 1.2352(14), Cu1-O2-C40 = 126.02(7), Cu1-O3-C1 = 125.24(8), Cu1-N1-C5 = 115.18(7), Cu1-N3-C3 = 119.16(8), Cu1-N3-C4 = 115.71(7), O2-Cu1-O3 = 88.66(7), O2-Cu1-N1 = 95.68(7), O2-Cu1-N3 = 175.080(8), O3-Cu1-N1 = 174.206(11), O3-Cu1-N3 = 95.81(7), N1-Cu1-N3 = 79.72(7), Cu1-N1-C31 = 122.66(8).

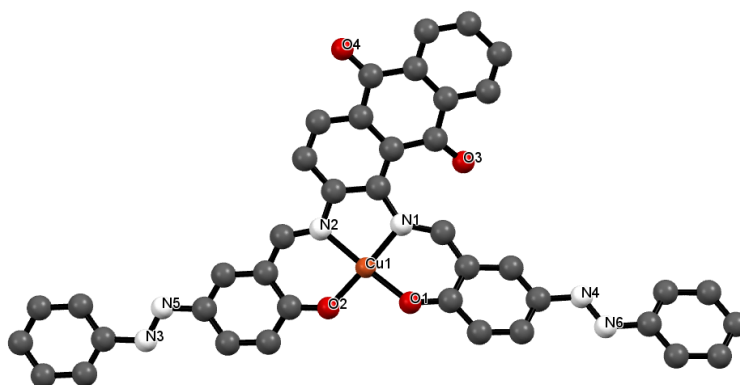


Figure 4. Crystal structure of **2** showing a selected atom labeling scheme. Selected bond lengths [Å] and angles [°] are as follows: Cu1-O1 = 1.975(3), Cu1-O2 = 1.855(3), Cu1-N1 = 1.929(3), Cu1-N2 = 2.040(4), N3-N5 = 1.237(2), N4-N6 = 1.336(2), Cu1-O1-C32 = 132.03(9), Cu1-O2-C40 = 128.92(11), Cu1-N2-C2 = 129.49(10), Cu1-N1-C5 = 108.02(12), Cu1-N2-C4 = 111.01(13), O1-Cu1-O2 = 93.35(13), O1-Cu1-N1 = 91.60(13), O1-Cu1-N2 = 175.792(9), O2-Cu1-N1 = 171.321(17), O2-Cu1-N2 = 88.64(13), N1-Cu1-N2 = 86.90(13), Cu1-N1-C3 = 119.52(11).

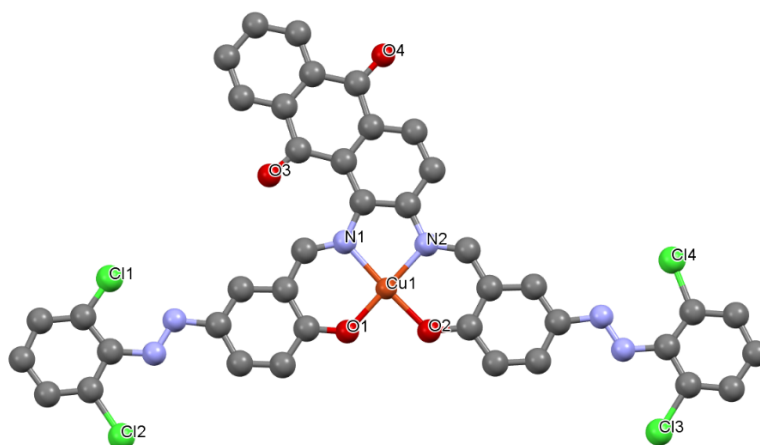


Figure 5. Crystal structure of **3** showing a selected atom labeling scheme. Selected bond lengths [Å] and angles [°] are as follows: Cu1-O1 = 1.9057(7), Cu1-O2 = 1.9386(8), Cu1-N1 = 1.9574(8), Cu1-N2 = 2.0150(8), N3-N3 = 1.2798(5), N5-N6 = 1.2794(5), Cu1-O1-C36 = 126.37(3), Cu1-O2-C35 = 128.31(2), Cu1-N2-C10 = 111.81(2), Cu1-N1-C27 = 124.98(3), Cu1-N2-C38 = 118.92(2), O1-Cu1-O2 = 93.35(13), O1-Cu1-N1 = 176.590(2), O1-Cu1-N2 = 94.63(3), O2-Cu1-N1 = 92.35(3), O2-Cu1-N2 = 171.250(4), N1-Cu1-N2 = 82.30(3), Cu1-N2-C39 = 112.58(3).

3.2. Spectral Characterization of Complexes

IR spectra for **1–3** exhibited characteristic and strong imine C = N bands around 1600 cm^{-1} for the Schiff base metal complexes. Slight shifts of these bands may be attributed to electronic aspects of the ligand of the complexes because the coordination geometries of the complexes are similar to each other [17,36].

Electronic, UV-vis (ultraviolet-visible) spectra for **1–3** in DMSO solutions displayed two $\pi\text{-}\pi^*$ bands around 250–350 nm and a $n\text{-}\pi^*$ band due to anthraquinone at about 480 nm. This is because the first absorption band ($n\text{-}\pi^*$ transition) of anthraquinone, which usually appears around 400 nm, experiences a shift to longer wavelength if it contains an electron donating substituent. The salen skeleton is formed or the metal includes an electron donating function [17]. Only **3** exhibited a considerable shift to longer wavelength. The qualitative assignments for **1** and **2** were also supported by DFT calculations (Table S1 and Figure 6). Obtaining agreeable data for **3** was difficult due to electron-withdrawing Cl-groups. The calculated DFT data for **1** for doublet ground states were as follows: energy = -2593.588 a.u. , alpha HOMO = -0.371 a.u. , LUMO = -0.357 a.u. , beta HOMO = -0.371 a.u. , and LUMO = -0.356 a.u. For **2**, on the other hand, the calculated data were as follows: energy = -2364.606 a.u. , alpha HOMO = -0.398 a.u. , LUMO = -0.335 a.u. , beta HOMO = -0.397 a.u. , and LUMO = -0.335 a.u.

To obtain the bonding pattern of the complexes, we generated density of state (DOS) and partial DOS (PDOS). The corresponding graphs are provided in Figure S2. The PDOS generated the frontier molecular orbitals of these complexes from the contribution of the metal and ligand orbitals. From Figure 6, it is evident that the HOMO (highest occupied molecular orbital) and LUMO (lowest unoccupied molecular orbital) for complex **1** are created by the mixture of Cu and ligand orbitals. Whereas, for complex **2**, the contribution is mainly related to the ligand. The metal contribution for complex **2** corresponds to higher unoccupied molecular orbitals like LUMO+3, LUMO+4, etc.

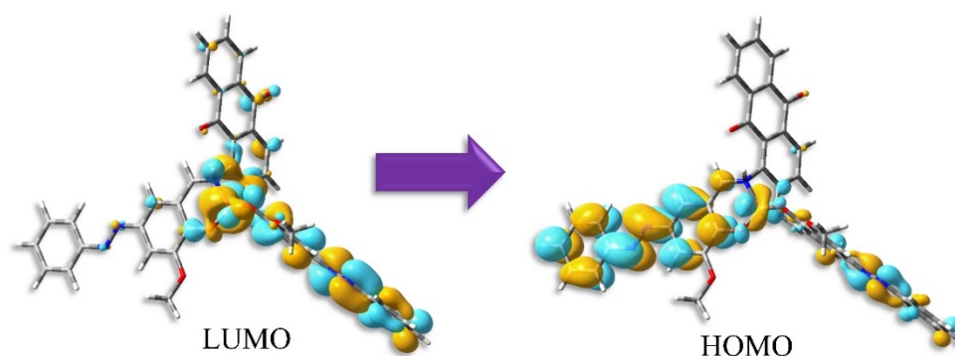


Figure 6. Distribution of HOMO and LUMO for *trans*-form of **1** by TD-DFT calculations.

Figure 7 exhibits the change of UV-vis spectra due to the *trans*- to *cis*-photoisomerization of azobenzene moiety of **1**, which displays a shift of π - π^* bands to a shorter wavelength [37]. The stable *trans*-form was converted to the *cis*-form by a metal-to-ligand charge transfer (MLCT) transition, whereby electrons move to the ligand (Figure 6), as well as other transitions, when irradiated by natural, namely unpolarized UV light [32,33]. Slow photoisomerization resulted in overlap of red and blue lines in Figure 7. Moreover, the reversible *cis*-*trans* photoisomerization, which converts the *cis*- to the *trans*-form by visible light irradiation, was observed for all complexes. However, the photoisomerization for **3** did not occur as smoothly when compared to that of **1** or **2**. Azobenzene dyes ending with electron-withdrawing or donor groups were reported to shift absorption or emission wavelengths and even affect photoisomerization [37,38]. Therefore, **1**, which exhibited the most efficient *cis*-*trans* photoisomerization, will mainly be discussed from here on.

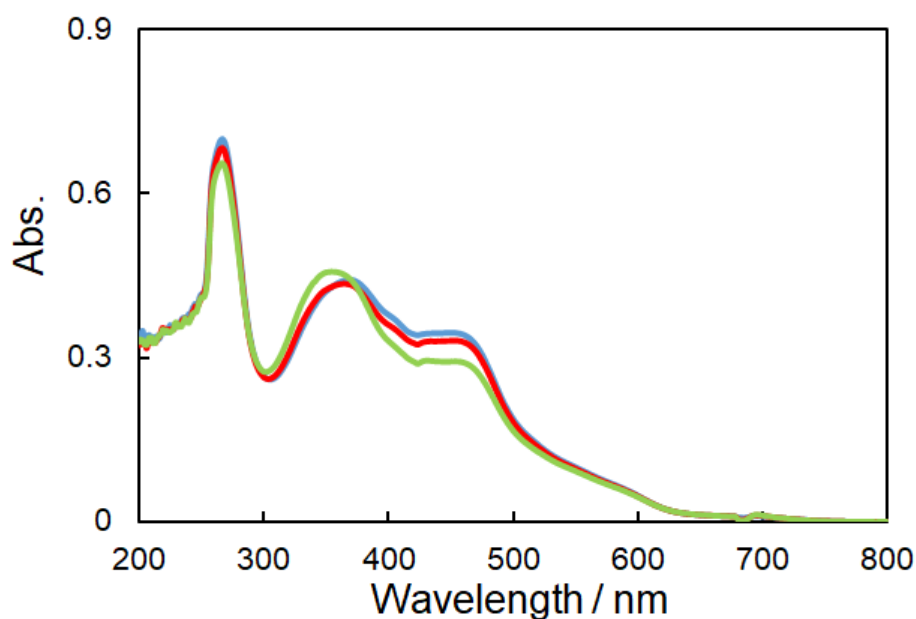


Figure 7. UV-vis spectra (DMSO solution) of **1** after UV light irradiation to yield the *cis*-form (Blue: 0 min, Red: 10 min, and Green: 20 min).

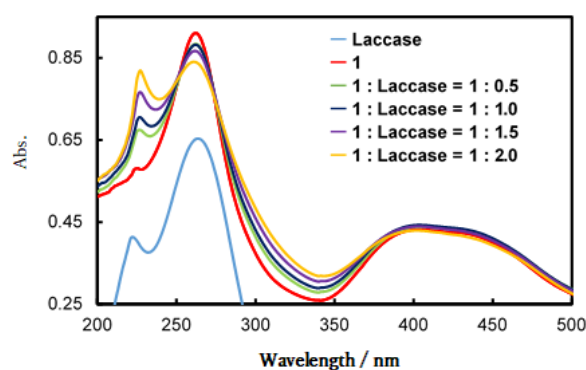
For a measurement of the angle-dependent polarized UV-vis absorption spectra at 320 nm, cast films were prepared by mixing a 5 wt% polymethyl methacrylate (PMMA) in DMF solution (PMMA: complex = 2:1). To evaluate the Weigert effect, we employed the *R* parameter to describe the degree of the photo-induced optical anisotropy [39–42].

$$R = \frac{A_0}{A_{90}} \quad (1)$$

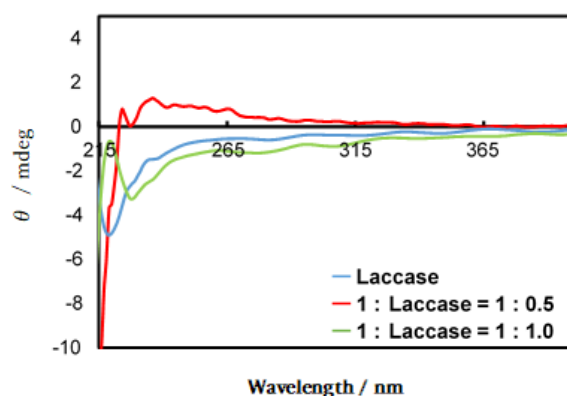
where A_{90} and A_0 denote the absorbance values measured with the measuring polarizer perpendicular or parallel to the direction of the electric vector of the irradiation of linearly polarized light. For polarized UV-vis spectra, completely isotropic chromophores are indicated by $R = 1$. Hence, the R parameter changes as the dichroism by alignment increases. The molecules in PMMA films were anisotropically oriented in the order of **2** ($R = 0.94$) > **1** ($R = 0.95$) > **3** ($R = 1.01$).

3.3. Spectra of Docking Cu Complex **1** and Laccase

Figure 8a shows UV-vis spectra (phosphate buffer at pH 7.3) of laccase, complex **1**, and spectral changes when laccase was added in 0.5, 1, 1.5, 2.0 equivalents to **1**, respectively. Pure laccase exhibited different spectrum than complexes excess ones, which may depend on associating features of two components resulting in induced CD. Adding laccase, an increase in the laccase-derived peak near 230 nm was observed. The most appropriate ratio of **1**: laccase according to Figure 8a was 1:1. As a result of the corresponding CD measurements (Figure 8b), a change was observed in the band at about 230 nm attributed to the α -helix helical structure, using a 1:1 ratio of **1**:laccase (their amounts were 6.0×10^{-6} mol) [16,19]. The CD spectrum of laccase agrees with analogous spectra reported for various types of laccase. Although no CD signals were expected for the achiral **1**, isolated (excess) **1** also exhibited a CD spectrum. The induced CD signals of **1** derived from chiral laccase molecules may be ascribed to a different spectrum [43–45].



(a)

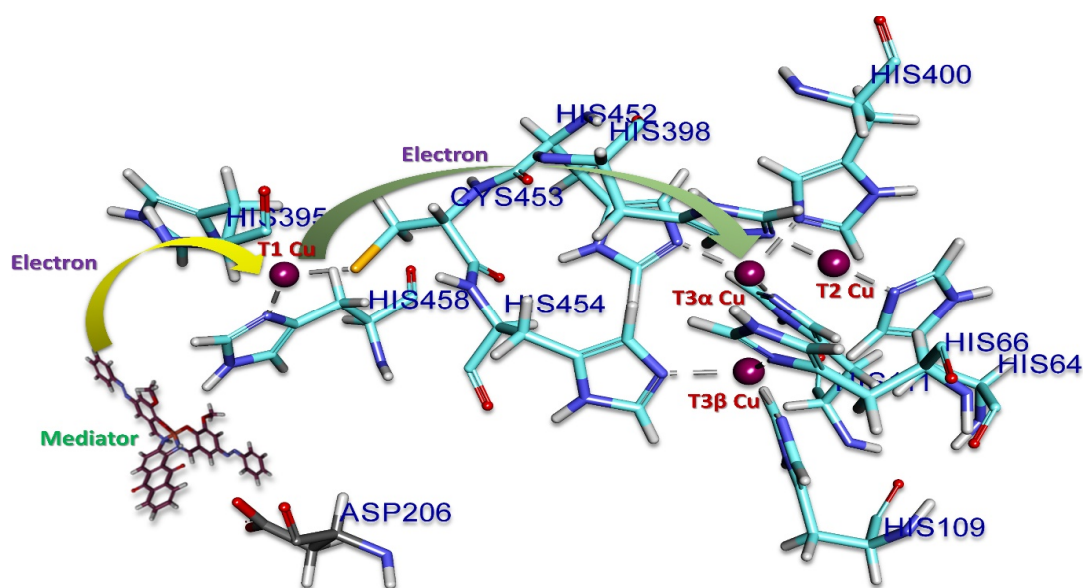


(b)

Figure 8. (a) Ultraviolet (UV)-vis and (b) circular dichroism (CD) spectra of variable ratios of laccase and **1** in a phosphate buffer.

Table 1. Bond distances and type between the laccase receptor and Complex 1.

Complex 1			
A:GLN242:HE22 - P:L1	1.10	Hydrogen Bond	Pi-Donor Hydrogen Bond
A:PRO396:HA - P:L1:O4	1.87	Hydrogen Bond	Carbon Hydrogen Bond
A:PHE239:HB1 - P:L1	2.05	Hydrophobic	Pi-Sigma
P:L1:H15 - P:L1:O1	2.21	Hydrogen Bond	Conventional Hydrogen Bond
A:ARG423:HD1 - P:L1:O6	2.24	Hydrogen Bond	Carbon Hydrogen Bond
P:L1:H18 - P:L1:O5	2.31	Hydrogen Bond	Carbon Hydrogen Bond
P:L1:H14 - P:L1:O1	2.35	Hydrogen Bond	Carbon Hydrogen Bond
A:ARG423:HH12 - P:L1:N3	2.87	Hydrogen Bond	Conventional Hydrogen Bond
A:SER427:HB2 - P:L1:O1	2.91	Hydrogen Bond	Carbon Hydrogen Bond
A:TYR244:OH - P:L1	2.93	Other	Pi-Lone Pair
P:L1 - A:VAL426	3.11	Hydrophobic	Pi-Alkyl
P:L1 - A:LEU451	3.63	Hydrophobic	Pi-Alkyl
P:L1 - A:ALA240	3.98	Hydrophobic	Pi-Alkyl
P:L1 - A:LEU399	4.01	Hydrophobic	Pi-Alkyl
P:L1 - A:ILE439	4.20	Hydrophobic	Pi-Alkyl
P:L1 - A:ALA240	4.48	Hydrophobic	Pi-Alkyl
P:L1 - A:ILE455	4.60	Hydrophobic	Pi-Alkyl
A:ARG423:NH2 - P:L1	4.65	Electrostatic	Pi-Cation
P:L1 - A:ILE382	4.76	Hydrophobic	Pi-Alkyl
P:L1 - A:ILE238	4.78	Hydrophobic	Pi-Alkyl
P:L1 - A:ALA240	4.90	Hydrophobic	Pi-Alkyl
P:L1 - A:VAL426	5.24	Hydrophobic	Pi-Alkyl

**Figure 10.** Representation of the mechanism on the active site of laccase. Copper (in violet) is involved in the electron transfer, stabilization, and orientation of the mediators. The surrounding amino acids are represented in sky blue. The mediator is in black and aspartic acid (206) is in grey.

3.5. Electrochemical Measurements for Docking Materials of Cu Complexes and Laccase

Electron transfer from mediator to copper sites are shown in Figure 10 in which redox properties of each metal site are important. Figure 11 shows the results of the cyclic voltammetry (CV) for 1–3. A glassy carbon (GC) electrode was used as a working electrode. The working electrode was prepared with respect to the following procedure. First, 5 mg of the complex was placed in 2 mL of acetone, mixed well with an ultrasonic cleaner, and then 40 μL dropped on the glassy carbon electrode and air-dried. The elution of the complex into the buffer solution was stopped by applying 10 μL of a 5 wt% Nafion[®] aliphatic alcohol-containing aqueous solution containing 45% of a conductive film (acetate buffer pH 5.0, 200 mM, scan 0.05 V/s) [14,16]. The oxidation potential derived from the central metal (copper) was observed in the range of 0 V, 0.1 to 0.2 V. For each complex, a significant current increase was confirmed after irradiation with linearly polarized UV light, which was attributed to changes in the electronic states of the complexes, switching from the *trans*-form to the *cis*-form.

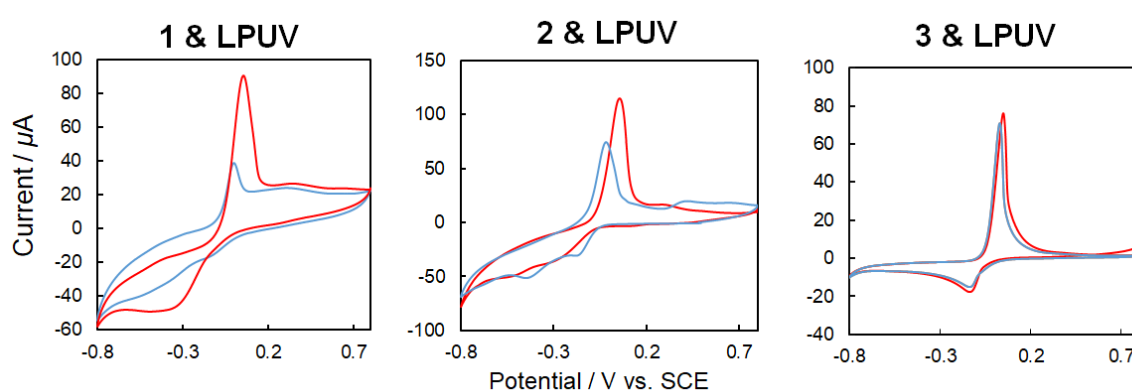


Figure 11. Cyclic voltammetry (CV) (50 mV/s, 200 mM acetate buffer, pH 5.0) for 1–3 (blue: *trans*-form, red, *cis*-form) before and after linearly polarized UV light irradiation for 3 min.

A laccase solution was prepared by dissolving 5 mg of laccase in 1 mL of ultrapure water and applied to 20 μL of the electrode. Then the electrode was dried. The elution of laccase into the buffer solution was stopped by applying 10 μL of a 5 wt% Nafion[®] aliphatic alcohol-containing aqueous solution containing 45% of a conductive film (acetate buffer pH 5.0, 200 mM, scan 0.05 V/s). In the case of CV using solely laccase (Figure 12 [top graphs]), laccase exhibited catalytic oxygen reduction under an oxygen purge. Furthermore, CV measurements were also performed for laccase and 1–3 as mediators (Figure 12 [bottom graphs]). In order to confirm the four-electron reduction of oxygen by laccase including mediators, CV measurements and comparisons were performed using an oxygen purge. For each of the complexes with inclusion of the mediator, an increase in the oxygen reduction peak was observed. The potential was positively shifted for 2 and 3, and the current was increased for 1 and 2.

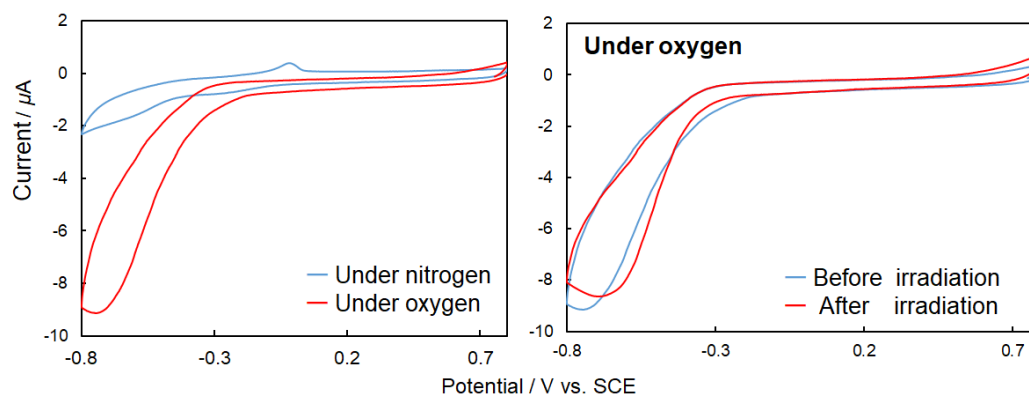


Figure 12. Cont.

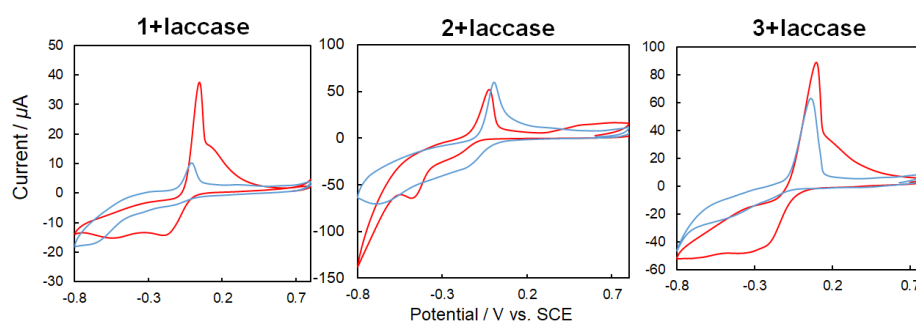


Figure 12. [Top graphs] Cyclic voltammetry (CV) (50 mV/s, 200 mM acetate buffer, pH 5.0) {right graph} for only laccase under nitrogen (blue) and oxygen purge (red) without ultraviolet (UV) light irradiation, {left graph} for laccase under oxygen purge before (blue) and after (red) natural UV light irradiation for 3 min. [Bottom graphs] CV (50 mV/s, 200 mM acetate buffer, pH 5.0) 1, 2 or 3 + laccase under nitrogen (blue) and oxygen purge (red) without UV light irradiation.

When unpolarized UV light was irradiated onto the hybrid materials of laccase and complexes 1–3 (Figure 13 (top)), CV changes occurred because of the differences in the electronic states of the *trans*-form and *cis*-form of the complexes induced by photoisomerization, as indicated in Figure 11. The differences in the complexes also affected the mediator performance. On the other hand, when irradiated with linearly polarized UV light (Figure 13 (bottom)), CV differences not only resulted from the *trans*-*cis* photoisomerization but also from irradiation with the non-polarized natural UV light. The latter difference could be attributed to the molecular orientation of the mediator complexes caused mainly by the Weigert effect. It was observed that the electron transfer between mediator to laccase can be controlled not only by the electronic states of the mediators but also by steric factors (spatial orientation and molecular docking). However, the path (through space or through bonds) and mechanism of the electron transfer is not clear because reaction rates [47–49] and spatial structures (such as chiral recognition) [50] could not be reliably explained with the present systems.

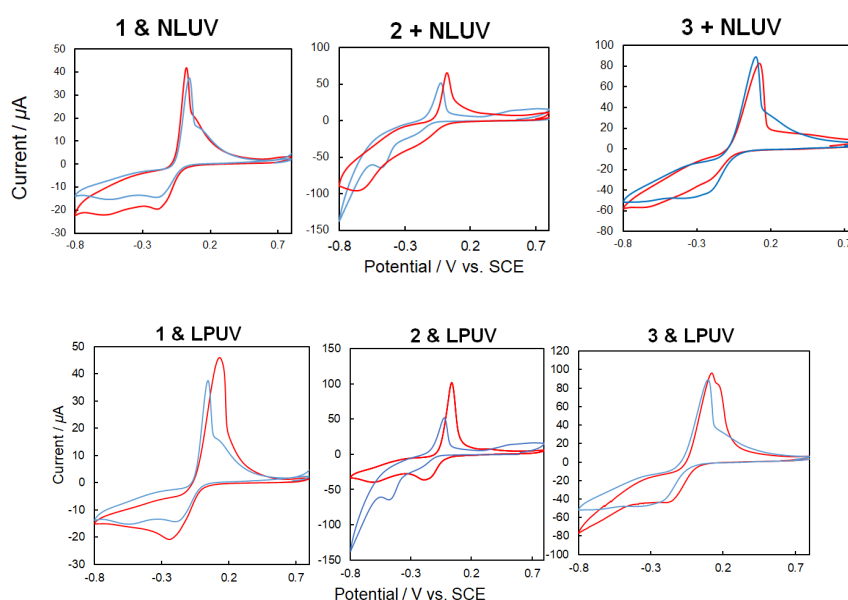


Figure 13. [Top] CV (50 mV/s, 200 mM acetate buffer, pH 5.0) of 1, 2 or 3 + laccase under oxygen purge before (blue) and after (red) natural UV light irradiation for 3 min. [Bottom] CV (50 mV/s, 200 mM acetate buffer, pH 5.0) of 1, 2 or 3 + laccase under oxygen purge before (blue) and after (red) linearly polarized UV light irradiation for 3 min.

The cathode reduction rate of biofuel cells depends on the efficiency of the long-range electron transfer process. To improve this electron transfer, several types of metal complexes were investigated as mediators between the electrode and laccase. The four copper atoms that are the active centers of the laccase are divided into three types (T1, T2, and T3) (α and β). The T2 copper and the two T3 copper form triple nuclear clusters. The T1 copper first receives electrons from the substrate and oxidizes the substrate, e.g., acting as a mediator in this case, which is followed by a four-electron reduction at T2 and T3 sites. A mediator is a substance sandwiched between an electrode and an enzyme that assists in donating and receiving electrons. Proposed docking sites were elucidated by computational simulation even though experiments exhibited changes of CV by irradiation of UV light, which occurred as both electronic changes and steric changes. Although intramolecular paths in laccase of electron transfer and electrochemical features of metal complexes were clear, the mechanism of electron transfer between metal complexes to laccase should be further understood.

The photochromic azobenzene moiety improves both the electronic structure and the steric orientation. Moreover, quinones (anthraquinone) and metal (Cu(II/I)) in the complexes can potentially be used as a mediator. Metalloproteins such as laccase can be regarded as metal complexes but have a complicated structure and complex ligands. In the case of phenolate, thiolate, oxo, sulfide, and *N*-heterocyclic chelates, the metal complex shows a very strong low-energy charge-transfer absorption band, which exhibited highly covalent ligand-metal bonds. These complexes are unique compared to the smaller copper complexes and exhibit spectral features derived from geometric and electronic structures of the metal ions resulting from the interaction with the protein biopolymers. Molecular docking of suitable compounds (both ligands and complexes) inside or on the surface of an enzyme with appropriate steric formation of the hydrophobic laccase pocket may be useful to predict their redox activity and suitability as biofuel cells. The present study suggested an experimental fact of salen-type mediator's molecular orientation dependence of electron transfer for the first time. Previous Mn paper [14] did not exhibit photo tuning of molecular orientation but effects due to photoisomerization.

These factors (electronic, steric, or spatial factors) contribute considerably to the electronic structure of the active site, which affected the geometry of the metal site, the orientation of the ligand-metal bond, and the conformation of the protein. Since the mediator not only influences the reaction rate of the enzyme but also the electron transfer rate, the selection of the optimum mediator and its better docking features is still one of the most important future research subjects.

4. Conclusions

In enzymatic fuel cells, the transfer of electrons between the enzyme and the electrode is an important issue to overcome and challenging to create and detection of hybrid materials. In this work, azo-anthraquinone salen Cu complexes were tested as a mediator for laccase. It was concluded from experiments that photo-tuning of electronic states and molecular orientation of the mediators resulted in differences of the electron transfer performance to laccase. Docking of achiral mediators to the surface of laccase (chiral protein) was confirmed and induced CD due to chiral environment. Docking simulation discussed the supramolecular interactions such as hydrogen bond and hydrophobic interaction.

There are several methods to directly deliver electrons into biofuel cells, such as using mediators or metal nanoparticles (having the advantage in spatial distance), or metal complexes (such as ferrocene and $[\text{Fe}(\text{CN})_6]^{3-/4-}$) [20] and organic molecules bound to the surface of protein molecules (having an advantage in current amounts). Besides these types of potential mediators or common organic mediators, the present azo-anthraquinone salen Cu complexes were confirmed to have advantage of photo-tuning their electronic states and spatial orientation. Among three complexes, 1 without disturbing substituent groups of electronic effects was comprehensively suitable for this purpose.

Even the theoretical studies can investigate electronic structures of photo-isomers at a molecular level. Experimental results herein also suggested that the electron transfer was related not only to electronic states but also reasonably to the molecular orientation [51,52]. Further studies are required to

specify the electron transfer mechanism and the electron path using appropriate experimental systems such as a modified electrode of laccase-mediator systems connected via enantiomers of oligopeptides.

Supplementary Materials: The following are available online at <http://www.mdpi.com/2073-8994/12/5/797/s1>, Figure S1: EPR spectra for powder samples of 2 and 3 at 300 K., Figure S2: PDOS with orbital contribution for 1 and 2, Figure S3: Comprehensive laccase receptor and copper complex interaction after docking. The copper complex is docked at the active site of the laccase receptor. The secondary structure of the laccase receptor is represented by the ribbon model, and the copper complex is represented by the stick model. Interactions of copper complex ligands (pink) with laccase receptor amino acids (sky blue) omitting the laccase receptor. The ligands surrounded by amino acids are represented in a three letter code marked in dark blue. a, b represents ligand 1, c, d represents ligand 2 and e, f represents ligand 3, Table S1: Summary of the results of DFT calculations for 1 and 2, Table S2: Bond distances and type between laccase receptor and Complex 2(L2) and Complex 3(L3).

Author Contributions: Conceptualization, T.A. Supervision, C.S. Experiments, K.K. Computation, S.P., R.P., S.G., and G.R. Writing Paper, S.P., T.H., and T.A. All authors have read and agreed to the published version of the manuscript.

Funding: This research received no external funding.

Acknowledgments: The XRD work was partly conducted at the Advanced Characterization Nanotechnology Platform of the University of Tokyo, and supported by the Nanotechnology Platform of the Ministry of Education, Culture, Sports, Science and Technology (MEXT), Japan.

Conflicts of Interest: The authors declare no conflict of interest.

References

1. Solomon, E.I.; Szilagyi, R.K.; DeBeer George, S.; Basumallick, L. Electronic structures of metal sites in proteins and models: Contributions to function in blue copper proteins. *Chem. Rev.* **2004**, *104*, 419–458. [[CrossRef](#)] [[PubMed](#)]
2. Quintanar, L.; Stoj, C.; Taylor, A.B.; Hart, P.J.; Kosman, D.J.; Solomon, E.I. Shall We Dance? How A Multicopper Oxidase Chooses Its Electron Transfer Partner. *Chem. Rev.* **2007**, *40*, 445–452.
3. Mate, D.M.; Alcalde, M. Laccase: A multi-purpose biocatalyst at the forefront of biotechnology. *Microbial Biotech.* **2017**, *10*, 1457–1467. [[CrossRef](#)] [[PubMed](#)]
4. Mano, N.; de Poulpique, A. O₂ Reduction in Enzymatic Biofuel Cells. *Chem. Rev.* **2018**, *118*, 2392–2468. [[CrossRef](#)]
5. Goff, A.; Holzinger, M.; Cosnier, S. Recent progress in oxygen-reducing laccase biocathodes for enzymatic biofuel cells. *Cell. Mol. Life Sci.* **2015**, *72*, 941–952. [[CrossRef](#)]
6. Moehlenbrock, M.J.; Minteer, S.D. Extended lifetime biofuel cells. *Chem. Soc. Rev.* **2008**, *37*, 1188–1196. [[CrossRef](#)]
7. Xiao, X.; Xia, H.-Q.; Wu, R.; Bai, L.; Yan, L.; Magner, E.; Cosnier, S.; Lojou, E.; Zhu, Z.; Liu, A. Tackling the Challenges of Enzymatic (Bio)Fuel Cells. *Chem. Rev.* **2019**, *119*, 9509–9558. [[CrossRef](#)]
8. Mehra, R.; Muschiol, J.; Meyer, A.S.; Kepp, K.P. A structural-chemical explanation of fungal laccase activity. *Sci. Rep.* **2018**, *8*, 17285. [[CrossRef](#)]
9. Morozova, O.V.; Shumakovich, G.P.; Shleev, S.V.; Yaropolov, Y.I. Laccase-Mediator Systems and Their Applications: A Review. *Appl. Biochem. Microbiol.* **2007**, *43*, 523–535. [[CrossRef](#)]
10. Sakai, H.; Mita, H.; Sugiyama, T.; Tokita, Y.; Shirai, S.; Kano, K. Construction of a Multi-stacked Sheet-type Enzymatic Biofuel Cell. *Electrochemistry* **2014**, *82*, 156–161. [[CrossRef](#)]
11. Hitaishi, V.P.; Clément, R.; Quattrocchi, L.; Parent, P.; Duché, D.; Zuily, L.; Ilbert, M.; Lojou, E.; Mazurenko, I. Interplay between Orientation at Electrodes and Copper Activation of *Thermus thermophilus* Laccase for O₂ Reduction. *J. Am. Chem. Soc.* **2020**, *142*, 1394–1405. [[CrossRef](#)] [[PubMed](#)]
12. Agbo, P.; Heath, J.R.; Gray, H.B. Modeling Dioxigen Reduction at Multicopper Oxidase Cathodes. *J. Am. Chem. Soc.* **2014**, *136*, 13882–13887. [[CrossRef](#)] [[PubMed](#)]
13. Cheng, C.-Y.; Liao, C.-I.; Lin, S.-F. Borate-fructose complex: A novel mediator for laccase and its new function for fructose determination. *FEBS Lett.* **2015**, *589*, 3107–3112. [[CrossRef](#)] [[PubMed](#)]
14. Kajiwara, K.; Yamane, S.; Haraguchi, T.; Pradhan, S.; Sinha, C.; Parida, R.; Giri, S.; Roymahaptra, G.; Moon, D.; Akitsu, T. Computational Design of Azo-anthraquinone Schiff Base Mn Complexes as Mediators for Biofuel Cell Cathode. *J. Chem. Chem. Eng.* **2019**, *13*, 23–33. [[CrossRef](#)]

15. Sano, A.; Yagi, S.; Haraguchi, T.; Akitsu, T. Synthesis of Mn (II) and, Cu (II) complexes including azobenzene and its application to mediators of laccase for biofuel cells. *J. Indian Chem. Soc.* **2018**, *95*, 487–494.
16. Kunitake, F.; Kim, J.-Y.; Yagi, S.; Yamazaki, S.; Haraguchi, T.; Akitsu, T. Chiral recognition of azo-Schiff base ligands, their Cu(II) complexes and their docking to laccase as mediators. *Symmetry* **2019**, *11*, 666. [[CrossRef](#)]
17. Mitsumoto, Y.; Sunaga, N.; Akitsu, T. Polarized light induced molecular orientation in laccase for chiral azosalen Mn(II), Co(II), Ni(II), Cu(II), Zn(II) mediators toward application for biofuel cell. *SciFed J. Chem. Res.* **2017**, *1*, 1.
18. Takeuchi, Y.; Akitsu, T. Anthraquinone Derivative Chiral Schiff Base Copper(II) Complexes for Enzyme Type Bio-Fuel Cell Mediators. *J. Electr. Eng.* **2016**, *4*, 189–195. [[CrossRef](#)]
19. Takeuchi, Y.; Sunaga, N.; Akitsu, T. Anthraquinone and L-amino Acid Derivatives Schiff Base Cu(II) Complexes as a Mediator between Cathode of Biofuel Cell and Oxygen-reducing Laccase. *Trend Green Chem.* **2017**, *3*, 1–8. [[CrossRef](#)]
20. Kurosawa, Y.; Tsuda, E.; Takase, M.; Yoshida, N.; Takeuchi, Y.; Mitsumoto, Y.; Akitsu, T. Spectroscopic and Electrochemical Studies on Metalloprotein (Laccase) and Cu(II) Complex Mediators As Model Systems for Biofuel Cell Cathodes. In *Threonine: Food Sources, Functions and Health Benefits*; Nova Science Publishers: Hauppauge, NY, USA, 2015; Chapter 4; pp. 73–86.
21. Natansohn, A.; Rochon, P. Photoinduced Motions in Azo-Containing Polymers. *Chem. Rev.* **2002**, *102*, 4139–4175. [[CrossRef](#)]
22. Shaw, S.; White, J.D. Asymmetric Catalysis Using Chiral Salen-Metal Complexes: Recent Advances. *Chem. Rev.* **2019**, *119*, 9381–9426. [[CrossRef](#)] [[PubMed](#)]
23. Routier, S.; Cotellet, N.; Catteau, J.-P.; Bernier, J.-L.; Waring, M.J.; Riou, J.-F.; Bailly, C. Salen-Anthraquinone Conjugates. Synthesis, DNA-Binding and Cleaving Properties, Effects on Topoisomerases and Cytotoxicity. *Bioorg. Med. Chem.* **1996**, *4*, 1185–1196. [[CrossRef](#)]
24. Roy, S.; Mondal, P.; Sengupta, P.S.; Dhak, D.; Santra, R.C.; Das, S.; Guin, P.S. Spectroscopic, computational and electrochemical studies on the formation of the copper complex of 1-amino-4-hydroxy-9,10-anthraquinone and effect of it on superoxide formation by NADH dehydrogenase. *Dalton Trans.* **2015**, *44*, 5428–5440. [[CrossRef](#)] [[PubMed](#)]
25. Kou, J.-F.; Qian, C.; Wang, J.-Q.; Chen, X.; Wang, L.-L.; Chao, H.; Ji, L.-N. Chiral ruthenium(II) anthraquinone complexes as dual inhibitors of topoisomerases I and II. *J. Biol. Inorg. Chem.* **2012**, *17*, 81–96. [[CrossRef](#)]
26. Yildiz, E.; Keles, M.; Kaya, A.; Dincer, S. Mononuclear Fe(III), Cr(III), Co(II) Metal Complexes Based on Azo-Anthraquinone Moieties: Synthesis, Characterizations and Antibacterial Activities. *Chem. Sci. Trans.* **2013**, *2*, 547–555. [[CrossRef](#)]
27. Kume, S.; Murata, M.; Ozeki, T.; Nishihara, H. Reversible Photoelectronic Signal Conversion Based on Photoisomerization-Controlled Coordination Change of Azobenzene-bipyridine Ligands to Copper. *J. Am. Chem. Soc.* **2005**, *127*, 490–491. [[CrossRef](#)]
28. Tylkowski, B.; Trojanowska, A.; Marturano, V.; Nowak, M.; Marciniak, L.; Giamberini, M.; Ambrogi, V.; Cerruti, P. Power of light-Functional complexes based on azobenzene molecules. *Coord. Chem. Rev.* **2017**, *351*, 205–217. [[CrossRef](#)]
29. Cárdenas-Moreno, Y.; Espinosa, L.A.; Vieyto, J.C.; González-Durruthy, M.; del Monte-Martinez, A.; Guerra-Rivera, G.; López, M.I.S. Theoretical study on binding interactions of laccase-enzyme from *Ganoderma weberianum* with multiples ligand substrates with environmental impact. *Ann. Proteom. Bioinform.* **2019**, *3*, 001–009.
30. Frisch, M.J.; Trucks, G.W.; Schlegel, H.B.; Scuseria, G.E.; Robb, M.A.; Cheeseman, J.R.; Scalmani, G.; Barone, V.; Mennucci, B.; Petersson, G.A.; et al. *Gaussian 09, Revision D.01*; Gaussian, Inc.: Wallingford, CT, USA, 2009.
31. Morris, G.M.; Huey, R.; Lindstrom, W.; Sanner, M.F.; Belew, R.K.; Goodsell, D.S.; Olson, A.J. Autodock4 and AutoDockTools4: Automated docking with selective receptor flexibility. *J. Comput. Chem.* **2009**, *16*, 2785–2791. [[CrossRef](#)]
32. Sato, H.; Beppu, I.; Haraguchi, T.; Akitsu, T.; Parida, R.; Giri, S.; Roymahapatra, G.; Joe, I.H. Optical properties of chiral Schiff base Mn(II), Co(II), Ni(II) complexes having azobenzene. *J. Indian Chem. Soc.* **2018**, *95*, 1487–1495.

33. Tanaka, S.; Sato, H.; Ishida, Y.; Deng, Y.; Haraguchi, T.; Akitsu, T.; Sugiyama, M.; Hara, M.; Moon, D. Photo-control of adsorption of dye metal complexes incorporating chiral Schiff base ligands containing azo-groups on TiO₂. *J. Korean Chem. Soc.* **2018**, *62*, 328–332.
34. Tsutsumi, Y.; Sunaga, N.; Haraguchi, T.; Akitsu, T. Induced CD from chiral Schiff base metal complexes involving azo-dye groups to gold nanoparticles. *J. Indian Chem. Soc.* **2017**, *94*, 1163–1172.
35. Yamaguchi, M.; Tsunoda, Y.; Tanaka, S.; Haraguchi, T.; Sugiyama, M.; Noor, S.; Akitsu, T. Molecular design through orbital and molecular design of new naphthyl-salen type transition metal complexes toward DSSC dyes. *J. Indian Chem. Soc.* **2007**, *94*, 761–772.
36. Onami, Y.; Kawasaki, T.; Aizawa, H.; Haraguchi, T.; Akitsu, T.; Tsukiyama, K.; Palafox, M.A. Degradation of human serum albumin by infrared free electron laser enhanced by inclusion of a salen-type Schiff base Zn (II) complex. *Int. J. Mol. Sci.* **2020**, *21*, 874. [[CrossRef](#)]
37. Akitsu, T.; Itoh, T. Polarized spectroscopy of hybrid materials of chiral Schiff base cobalt(II), nickel(II), copper(II), and zinc(II) complexes and photochromic azobenzenes in PMMA films. *Polyhedron* **2010**, *29*, 477–487. [[CrossRef](#)]
38. Diana, R.; Panunzi, B.; Shikler, R.; Nabha, S.; Caruso, U. A symmetrical azo-based fluorophore and the derived salen multipurpose framework for emissive layers. *Inorg. Chem. Commun.* **2019**, *104*, 186–189. [[CrossRef](#)]
39. Diana, R.; Caruso, U.; Piotta, S.; Concilio, S.; Shikler, R.; Panunzi, B. Spectroscopic Behaviour of Two Novel Azobenzene Fluorescent Dyes and Their Polymeric Blends. *Molecules* **2020**, *25*, 1368. [[CrossRef](#)]
40. Kominato, C.; Akitsu, T. Photoinduced molecular orientation of catalytic-like chiral azo-Schiff base complexes in PMMA or laccase matrices. *Lett. Appl. Nanobiosci.* **2015**, *2*, 264–270.
41. Ito, M.; Akitsu, T.; Palafox, M.A. Theoretical interpretation of polarized light-induced supramolecular orientation on the basis of normal mode analysis of azobenzene as hybrid materials in PMMA with chiral Schiff base Ni(II), Cu(II), and Zn(II) complexes. *J. Appl. Solut. Chem. Model.* **2016**, *5*, 30–47.
42. Yamazaki, A.; Akitsu, T. Polarized spectroscopy and polarized UV light-induced molecular orientation of chiral diphenyl Schiff base Ni(II) and Cu(II) complexes and azobenzene in a PMMA film. *RSC Adv.* **2012**, *2*, 2975–2980. [[CrossRef](#)]
43. Kominato, C.; Akitsu, T. Computational Study on UV-Vis and CD Spectra of Chiral Schiff Base Ni(II), Cu(II), and Zn(II) Complexes for Discussion of Induced CD. *J. Chem. Chem. Eng.* **2012**, *6*, 199–208.
44. Akitsu, T.; Uchida, N.; Aritake, Y.; Yamaguchi, J. Induced d-d Bands in CD Spectra due to Chiral Transfer from Chiral Nickel(II) Complexes to Achiral Copper(II) Complexes and Application for Structural Estimation. *Trends Inorg. Chem.* **2018**, *10*, 41–49.
45. Akitsu, T.; Uchida, N. Induced d-d bands in CD spectra of solution of chiral Schiff base nickel(II) complex and ferrocene. *Asian Chem. Lett.* **2010**, *14*, 21–28.
46. Piontek, K.; Antorini, M.; Choinowski, T. Crystal Structure of a Laccase from the Fungus *Trametes versicolor* at 1.90-Å Resolution Containing a Full Complement of Coppers. *J. Biol. Chem.* **2002**, *277*, 37663–37669. [[CrossRef](#)]
47. Lappin, A.G.; Segal, M.G.; Weatherburn, D.C.; Sykes, A.G. Kinetic Studies on 1:1 Electron-Transfer Reactions Involving Blue Copper Proteins. 2. Protonation Effects and Different Binding Sites in the Oxidation of Parsley Plastocyanin with Co(4,7-DPSphen)₃³⁺, Fe(CN)₆³⁻, and Co(phen)₃³⁺. *J. Am. Chem. Soc.* **1979**, *101*, 2298–2301. [[CrossRef](#)]
48. Chapman, S.K.; Knox, C.V.; Sykes, A.G. Kinetic studies on 1:1 electron-transfer reactions involving blue copper proteins. Part 10. The assignment of binding sites in the reactions of plastocyanin (and azurin) with non-physiological protein redox partners. *J. Chem. Soc. Dalton Trans.* **1984**, 2775–2780. [[CrossRef](#)]
49. Effects, Protein-Complex Association, and Binding Sites in Reactions of *Pseudomonas aeruginosa* Azurin with Co(phen)₃³⁺, Co(4,7-DPSphen)₃³⁻, and Fe(CN)₆³⁻ (Oxidants) and Fe(CN)₆⁴⁻ (Reductant). *J. Am. Chem. Soc.* **1979**, *101*, 2302–2306. [[CrossRef](#)]
50. Nazmutdinov, R.R.; Bronshtein, M.D.; Zinkicheva, T.T.; Hansen, N.S.; Zhang, J.; Ulstrup, J. Chiral Selectivity in Inter-reactant Recognition and Electron Transfer of the Oxidation of Horse Heart Cytochrome *c* by Trioxalatocobaltate(III). *Inorg. Chem.* **2016**, *55*, 9335–9345. [[CrossRef](#)]

51. Siders, P.; Cave, R.J.; Marcus, R.A. A model for orientation effects in electrontransfer Reactions. *J. Chem. Phys.* **1984**, *81*, 5613–5624. [[CrossRef](#)]
52. Domingue, R.P.; Fayer, M.D. Influence of Orientational Fluctuations on Electron Transfer in Systems of Donor-Acceptor Pairs. *J. Phys. Chem.* **1986**, *90*, 5141–5146. [[CrossRef](#)]



© 2020 by the authors. Licensee MDPI, Basel, Switzerland. This article is an open access article distributed under the terms and conditions of the Creative Commons Attribution (CC BY) license (<http://creativecommons.org/licenses/by/4.0/>).